PERSPECTIVE

Check for updates

Vacancy defect tuning of electronic structures of transition metal (hydr)oxide-based electrocatalysts for enhanced oxygen evolution

Cheng-Zong Yuan, [ID] [a] Siyu Huang,[a] Hongrui Zhao,[a] Jiang Li,[a] Lunliang Zhang,[a] Yao Weng,[a] Tuck-Yun Cheang,*[b] Hong Yin, [ID] *[c] Xiaomeng Zhang*[ade] and Shufeng Ye[de]

Electrocatalytic water splitting has already been regarded as a promising approach to generate pure hydrogen (H_2) and oxygen (O_2). However, the oxygen evolution reaction (OER) occurring at the anode during water splitting is very sluggish, because it involves four-electron oxidation steps. Therefore, developing highly efficient and cost-effective electrocatalysts to accelerate its reaction rate and lower its reaction barrier is of great significance, but still remains a big challenge. Strikingly, transition metal (hydr)oxide-based electrocatalysts have attracted wide research interest owing to their high intrinsic activity and low-cost feature. Unfortunately, these transition metal (hydr)oxide-based electrocatalysts always suffer from relatively low conductivity. To address this problem, some efficient strategies have been reported to enhance their conductivity by tuning the electronic structures, further boosting their performances. In this review, three state-of-the-art defect-tuning strategies, including oxygen vacancy defects, metal cation vacancy defects and multivacancy defects, for boosting the OER performances of transition metal (hydr)oxide-based electrocatalysts are summarized. It is found that defects can rationally regulate the electronic structures of transition metal (hydr)oxide-based electrocatalysts, improve the conductivity, optimize the adsorption ability with intermediates and lower the reaction energy barrier of the OER, consequently enhancing their electrocatalytic performances. These defect-tuning strategies open a new avenue for boosting the electrocatalytic performances of low-cost transition metal (hydr)oxide-based nanomaterials, making them promising candidates for replacinge noble metal catalysts for large-scale electrochemical water splitting.

1. Introduction

Owning to the global environmental issues and limited reserves of fossil fuels, finding renewable clean energy resources has attracted extensive research interest. Hydrogen (H_2) as an ecofriendly and sustainable energy carrier is one of the most promising alternatives to replace conventional fossil fuels in the future.[1–3] Among the approaches employed for producing H_2, electrocatalytic water splitting technology ($2H_2O_{(l)} = 2H_{2(g)} +$

$O_{2(g)}$) powered by sustainable electricity as shown in Fig. 1 exhibits tremendous potential for generating pure H_2 with high energy conversion efficiency.[4–6] Electrocatalytic water electrolysis involves two half reactions: the hydrogen evolution reaction (HER) at the cathode and the oxygen evolution reaction (OER) at the anode.[7–9] The HER is a two-electron transfer process ($2H^+_{(aq)} + 2e^- = H_{2(g)}$), while the OER at the anode involves four-electron oxidation steps, which is more sluggish than the HER, thus leading to high overpotential of water splitting.[10–12] Therefore, to accelerate the reaction rate and lower the over-potential of water splitting, highly effective and stable OER electrocatalysts are usually needed for water electrolysis. At present, the state-of-the-art electrocatalysts for the OER are IrO_2, RuO_2 and their related compounds.[13] However, these noble metal-based electrocatalysts suffer from the drawbacks of high cost and scarcity, seriously restricting their large-scale applications. Therefore, design and synthesis of highly efficient, durable and low-cost electrocatalysts for electrocatalyzing the OER have become an imperative and challenging topic. Until now, numerous efforts have already been made to develop efficient and stable OER

[a] Jiangxi Province Key Laboratory of Cleaner Production of Rare Earths, Ganjiang Innovation Academy, Chinese Academy of Sciences, Ganzhou 341119, China. E-mail: xmzhang@gia.cas.cn

[b] The First Affiliated Hospital of Clinical Medicine of Guangdong Pharmaceutical University, Guangdong, 510080, P. R. China. E-mail: 13631322559@163.com

[c] International Iberian Nanotechnology Laboratory (INL), Av. Mestre Jose Veiga, 4715-330 Braga, Portugal. E-mail: 2017507027@hust.edu.cn

[d] State Key Laboratory of Multiphase Complex Systems, Institute of Process Engineering, Chinese Academy of Sciences, PO Box 353, Beijing 100190, China

[e] Center of Materials Science and Optoelectronics Engineering, University of Chinese Academy of Sciences, Beijing 100049, China
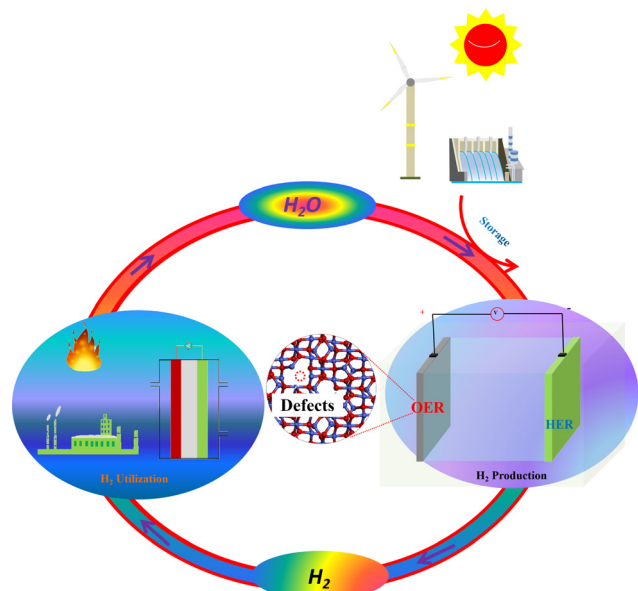
Fig. 1 Electrocatalytic water splitting powered by renewable energies to produce H_2 and the utilization of H_2.

electrocatalysts utilizing earth-abundant elements. For example, Liu *et al.* prepared Co_3O_4 with different morphologies by solution, hydrothermal and sol–gel methods.[14] It was found that Co_3O_4 with urchin-like structures is beneficial for the OER owing to its high ability of detaching O_2 bubbles from the interfaces. Wang *et al.* synthesized Co_3S_4/NCNTs consisting of cobalt sulfide immobilized on nitrogen-doped carbon nanotubes (NCNTs) *via* an anion-exchange method.[15] The as-prepared Co_3S_4/NCNT electrocatalyst exhibited good activities towards the OER with an overpotential of 430 mV at a current density of 10 mA cm^{-2} in 0.1 M KOH. Yu's group reported an NG-$CoSe_2$ electrocatalyst containing $CoSe_2$ nanobelts supported by nitrogen-doped reduced graphene oxides.[16] In 0.1 M KOH, this NG-$CoSe_2$ material exhibited an overpotential of mere 366 mV at a current density of 10 mA cm^{-2} and a small Tafel slope of 40 mV dec^{-1}, which is comparable to that of the commercial RuO_2 electrocatalyst. Wang's group fabricated a CoP/C electrocatalyst with sandwich-like structures through a low-temperature phosphorization approach.[17] As a stable OER catalyst, the as-obtained CoP/C showed a small overpotential of only 330 mV at a current density of 10 mA cm^{-2} in 1 M KOH. Moreover, phosphorus-doped few-layer graphene (G-P) as a metal-free OER electrocatalyst was synthesized by simply ball-milling graphite and red phosphorus.[18] The obtained G-P electrocatalyst needed a small overpotential of 330 mV to achieve a current density of 10 in 1 M KOH. Up to now, we know that transition metal (hydr)oxide-based nanomaterials among the various OER electrocatalysts have attracted wide research attention, due to their high intrinsic electrocatalytic performances. Besides, the earth abundance, ultra-stability and low-toxicity of transition metal (hydr)oxide-based materials also make them promising as OER electrocatalysts. Although these transition metal (hydr)oxide-based nanomaterials show good OER performances, they usually suffer from relatively low conductivity. Therefore, to efficiently address this problem,

some potential strategies have been reported to tune their electronic structure and further enhance their conductivity.[19–24]

Recently, introducing vacancy defects into metal (hydr)-oxide-based nanomaterials has been reported as a promising method to improve the conductivity. It was found that vacancy defects can rationally regulate the electronic structures of transition metal (hydr)oxide-based electrocatalysts, thus improving their conductivity. Moreover, the adsorption ability with intermediates over the surfaces of transition metal (hydr)oxide-based electrocatalysts could also be optimized, leading to lower reaction energy barriers. In this work, vacancy defects including oxygen vacancy defects, metal cation vacancy defects and multivacancy defects for enhancing the OER performances of transition metal (hydr)oxide-based electrocatalysts are summarized, which may make them highly efficient candidates for replacing noble metal catalysts for large-scale electrochemical water splitting.

2. Oxygen evolution reaction

The OER at the anode in water electrolysis involves a four-electron oxidation process, which is more complex and sluggish than the HER. To trigger the OER, efficient oxygen evolution electrocatalysts are generally employed, and an external potential larger than the theoretical voltage (called overpotential) is needed.[25–28] Subsequently, the large overpotential and sluggish kinetics of the OER mainly impede the development of water splitting technology. On this account, it is of great importance to synthesize highly efficient OER electrocatalysts to lower its reaction barrier and accelerate the reaction rate. Understanding the catalytic mechanism of the OER is very instructive and meaningful to design advanced electrocatalysts or boost the performances of existing electrocatalysts.[29–33] It is widely recognized that the OER follows different reaction mechanisms in different electrolytes. When an alkaline solution is employed as the electrolyte, the reaction equation will be $4OH^- = 2H_2O + 4e^- + O_2$, and the possible reaction steps are shown in Table 1, where * represents the active site on electrocatalyst surfaces.[34–38] The first step of the reported reaction mechanisms in an alkaline electrolyte is adsorption and activation of the OH^- species at the active site. After that, different intermediate reaction steps occur depending on the electrocatalysts. The intermediate reaction step with the highest reaction barrier is regarded as the rate-determining step, which determines the overpotential of the OER. For excellent electrocatalysts, the free energies in each elemental step will be similar.[33] In 1984, S. Trasatti, reported a volcano plot of transition metal oxide electrodes for the OER, in which RuO_2 and IrO_2 were located at the top of the plot due to their intrinsic electronic structures and outstanding adsorption of oxygen-based intermediates.[38] Therefore, engineering the electronic structures of low-cost transition metal (hydr)oxide-based nanomaterials for greatly boosting their performances to replace noble metal-based electrocatalysts is of great significance.

In acidic or neutral solution, the reaction equation is $2H_2O = 4H^+ + 4e^- + O_2$, and the corresponding reaction steps are

Table 1   OER elementary reaction steps over oxides in alkaline media

Reaction mechanisms	Elementary reaction steps
Electrochemical oxide path[34]	(a) $* + OH^- \rightarrow *\text{–}OH + e^-$ (b) $*\text{–}OH + OH^- \rightarrow *\text{–}O + H_2O + e^-$ (c) $2*\text{–}O \rightarrow 2* + O_2$
Oxide path[34]	(a) $* + OH^- \rightarrow *\text{–}OH + e^-$ (b) $2*\text{–}OH \rightarrow *\text{–}O + * + H_2O$ (c) $2*\text{–}O \rightarrow 2* + O_2$
Krasil'shchkov path[35]	(a) $* + OH^- \rightarrow *\text{–}OH + e^-$ (b) $*\text{–}OH + OH^- \rightarrow *\text{–}O^- + H_2O$ (c) $*\text{–}O^- \rightarrow *\text{–}O + e^-$ (d) $2*\text{–}O \rightarrow 2* + O_2$
Yeager's path[36,37]	(a) $* + OH^- \rightarrow *\text{–}OH + e^-$ (b) $*^z\text{–}OH \rightarrow *^{z+1}\text{–}OH + e^-$ (c) $2*^{z+1}\text{–}OH + 2OH^- \rightarrow 2* + 2H_2O + O_2$
Bockris path[38]	(a) $* + OH^- \rightarrow *OH + e^-$ (b) $*OH + OH^- \rightarrow *\text{–}H_2O_2 + e^-$ (c) $*\text{–}H_2O_2 + OH^- \rightarrow *\text{–}O_2H^- + H_2O$ (d) $*\text{–}H_2O_2 + *\text{–}O_2H^- \rightarrow 2* + H_2O + OH^- + O_2$

summarized in Table 2, in which * represents the active site of electrocatalysts.[34,35,39,40] In general, the most accepted reaction steps in acidic media are the electrochemical oxidation path and the oxidation path. For all the reaction mechanisms in acidic media, the initial step is the adsorption of H_2O molecules and the breaking of O–H bonds. Because of strong covalent O–H bonds, higher overpotential is needed to trigger the OER process in acid solution, and the reaction rate is more sluggish than that of the alkaline OER process.[41,42] Following that, different intermediate steps are observed in diversified reaction mechanisms. Moreover, the electrocatalysts may undergo reconstruction during the OER under practical working conditions, which makes it hard to get a deep insight into the reaction mechanisms. At present, in situ characterization techniques can help efficiently monitor the surface oxidation state and detect the local atomic-structure transformation, which have been useful methods for understanding the reaction mechanism and identifying the catalytically active sites.[43–52]

3. Tuning of (hydr)oxide-based electrocatalysts with defects

As is known, the defects include vacancies, lattice strain, dislocation, grain boundaries, and so on. Generally, the charge distribution, band structure, e_g electron filling, and spin

transition of electrocatalysts could be regulated via different defects.[53–58] Therefore, introducing defects into electrocatalysts is an efficient approach for boosting the intrinsic activity. In this section, three defect-regulating strategies, including oxygen vacancy defects, metal cation vacancy defects and multivacancy defects, are summarized for boosting the OER performances of transition metal (hydr)oxide-based electrocatalysts.

3.1 Oxygen vacancy defects

Oxygen vacancies with low formation energy are one of the common anion defects in transition metal-based (hydr)oxides.[59] The electronic structures of electrocatalysts could be regulated via the introduction of oxygen vacancy defects; therefore, introducing oxygen vacancies into (hydr)oxide-based electrocatalysts has been widely employed for enhancing their electrocatalytic performances in the past years. To introduce oxygen vacancy defects into transition metal-based (hydr)oxides, efficient synthesis strategies (such as $NaBH_4$ solution reduction, solvothermal reduction, radiofrequency plasma treatment and calcination treatment under a H_2/Ar atmosphere) are developed and always employed. For example, Zheng's group presented a facile method (shown in Fig. 2a) for preparing oxygen vacancy-rich Co_3O_4 nanowires using aqueous $NaBH_4$ as a reducing agent.[60] The scanning electron microscopy (SEM) image in Fig. 2b shows that the as-obtained oxygen vacancy-rich Co_3O_4 nanowires have

Table 2   OER elementary reaction steps over oxides in acidic media

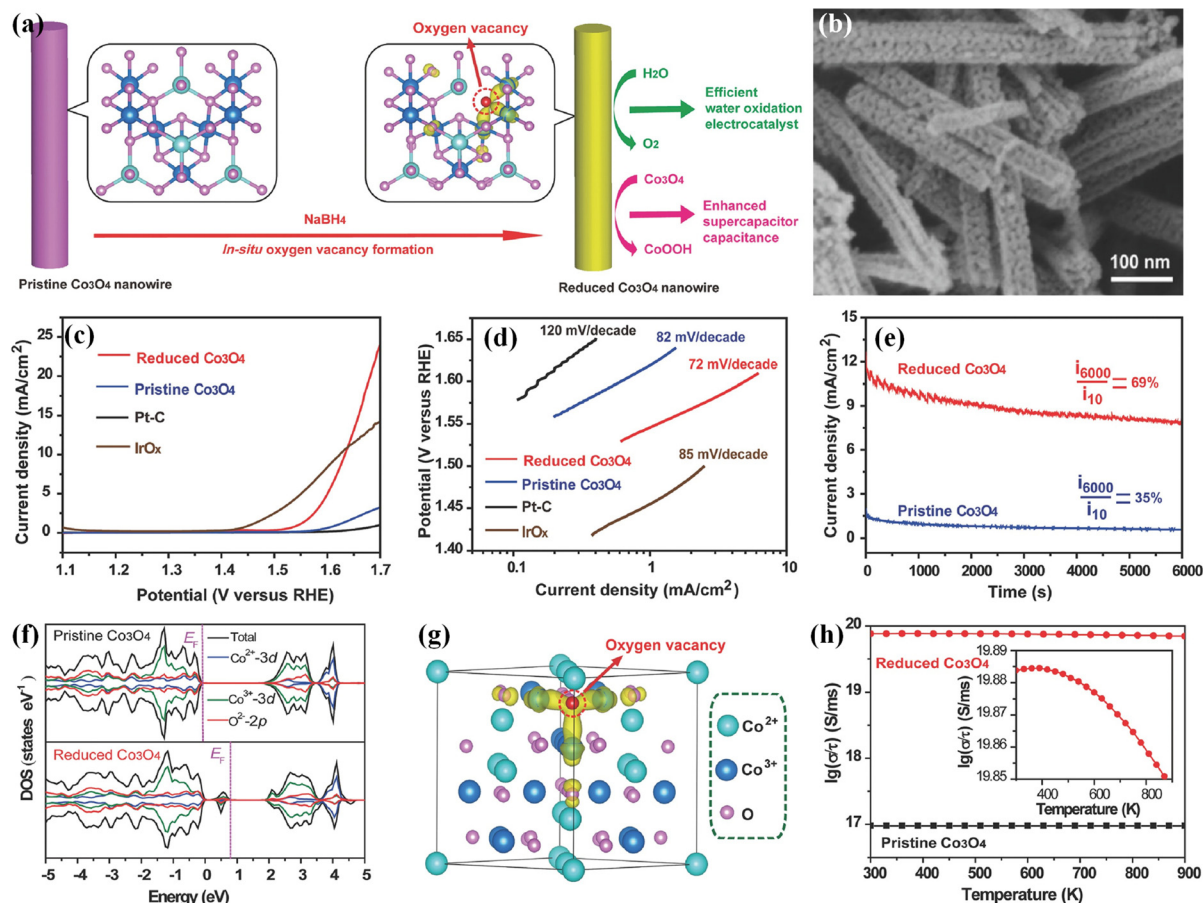| Reaction mechanisms	Elementary reaction steps
Electrochemical oxide path[34]	(a) $* + H_2O \rightarrow *\text{–}OH + H^+ + e^-$ (b) $*\text{–}OH \rightarrow *\text{–}O + H^+ + e^-$ (c) $2*\text{–}O \rightarrow 2* + O_2$
Oxide path[34]	(a) $* + H_2O \rightarrow *\text{–}OH + H^+ + e^-$ (b) $2*\text{–}OH \rightarrow *\text{–}O + * + H_2O$ (c) $2*\text{–}O \rightarrow 2* + O_2$
Krasil'shchkov path[35]	(a) $* + H_2O \rightarrow *\text{–}OH + H^+ + e^-$ (b) $*\text{–}OH \rightarrow *\text{–}O^- + H^+$ (c) $*\text{–}O^- \rightarrow *\text{–}O + e^-$ (d) $2*\text{–}O \rightarrow 2* + O_2$
Wade and Hackerman's path[40]	(a) $2* + 2H_2O \rightarrow *O + *H_2O + 2H^+ + 2e^-$ (b) $*O + 2*OH^- \rightarrow 2* + *H_2O + O_2 + 2e^-$

Fig. 2 (a) Schematic of introducing oxygen vacancy defects into Co_3O_4 nanowires. (b) SEM image of the obtained Co_3O_4 nanowires with oxygen vacancy defects. (c) LSV curves and (d) Tafel plots of the Co_3O_4 with oxygen vacancy defects, pristine Co_3O_4, IrO_x and Pt/C. (e) Stability of Co_3O_4 with oxygen vacancy defects and pristine Co_3O_4 in 1 M KOH. (f) TDOS and PDOSs of Co_3O_4 with or without oxygen vacancies. (g) Partial charge density of Co_3O_4 with oxygen vacancies. (h) Conductivities of the Co_3O_4 with or without oxygen vacancies.[60] Copyright 2014, Wiley-VCH.

the same morphology as that of pristine Co_3O_4, indicating that the morphology structure features are well preserved after $NaBH_4$ reduction. The X-ray diffraction (XRD) patterns demonstrate that oxygen vacancy-rich Co_3O_4 nanowires are still well indexed to cubic Co_3O_4, indicating the preservation of crystal structure features. The X-ray photoelectron spectroscopy (XPS) results display new satellite peaks attributed to the Co^{2+} oxidation state in oxygen vacancy-rich Co_3O_4, suggesting that a portion of Co^{3+} has been reduced to Co^{2+} and oxygen vacancies have been formed. Linear sweep voltammetric (LSV) curves in Fig. 2c show that the onset overpotential of the as-obtained oxygen vacancy-rich Co_3O_4 nanowires is about 290 mV, which is 50 mV lower than that of pristine Co_3O_4 and its specific activity is 7 times higher than that of pristine Co_3O_4 at 1.65 V. Tafel plots in Fig. 2d display a low Tafel slope of 72 mV dec^{-1} for oxygen vacancy-rich Co_3O_4 nanowires, suggesting a more facile charge transfer after introducing oxygen vacancies. Moreover, the stability of pristine Co_3O_4 and the oxygen vacancy-rich Co_3O_4 nanowires is evaluated via chronoamperometric measurements (Fig. 2e), and the results further demonstrate that oxygen vacancies can also improve the durability of Co_3O_4 electrocatalysts. To explore the effect of oxygen vacancy defects on the

electronic structures and electrocatalytic performances of Co_3O_4, density-functional theory (DFT) calculations are employed. Fig. 2f exhibits the total densities of states (TDOSs) and the projected densities of states of states (PDOSs) of Co_3O_4 with or without oxygen vacancies. The calculated results demonstrate that new states are generated within the band gap after introducing oxygen vacancies. The calculated partial charge density in Fig. 2g shows that oxygen vacancy-rich Co_3O_4 possesses more delocalized electrons than perfect Co_3O_4. Furthermore, the corresponding conductivity (Fig. 2h) of oxygen vacancy-rich Co_3O_4 with metal characteristics is much better than that of perfect Co_3O_4 semiconductors. These results demonstrate that the oxygen vacancies could lead to new gap states and electron delocalization, which greatly improve the conductivity and further drastically boost the electrocatalytic OER activities of Co_3O_4. Moreover, introducing oxygen vacancies can also contribute to an enhanced stability of the Co_3O_4 catalyst. Zhu et al. further illustrated that $NaBH_4$ possesses strong reducing capacity; therefore, the $NaBH_4$ reduction approach has been an efficient strategy for introducing oxygen vacancies into transition metal-based (hydr)oxide electrocatalysts to boost their electrocatalytic OER activity and stability.[61,62]

Afterward, Sun's group reported a solvothermal reduction method (Fig. 3a) for preparing single-crystalline Co_3O_4 nanosheets with oxygen vacancies using ethylene glycol as the reducing agent.[63] DFT calculations revealed that the bandgap of oxygen vacancy-rich Co_3O_4 is about 1.74 eV, which is lower than that of perfect Co_3O_4, demonstrating that oxygen vacancies can improve the conductivity. Moreover, oxygen atoms in Co_3O_4 work as active sites for the OER, which gives rise to a large overpotential of about 2.46 eV (Fig. 3b), while Co atoms in the oxygen vacancy-rich Co_3O_4 are exposed and serve as the real active sites for the OER, which could greatly lower the reaction barrier (2.26 eV). To investigate the oxygen vacancy defects in the as-prepared Co_3O_4, XPS measurements and X-ray absorption spectroscopy (XAS) were carried out. As shown in Fig. 3c, enrichment of O-vacancies was clearly observed in the O 1s XPS spectrum of the obtained oxygen vacancy-rich Co_3O_4 nanosheets, suggesting that more oxygen vacancies were created on the surface of Co_3O_4 by this solvothermal reduction method.

The Co K-edge X-ray absorption near edge structure (XANES) shown in Fig. 3d displays that the Co valence state in the oxygen vacancy-rich Co_3O_4 nanosheets is lower than that in Co_3O_4 because of the existence of O-vacancy defects. In the extended X-ray absorption fine structure (EXAFS) spectrum (Fig. 3e), it can be found that the peak intensity of oxygen vacancy-rich Co_3O_4 nanosheets becomes lower, further suggesting the existence of oxygen vacancies. The Fourier-transformed data in Fig. 3f reveals that Co coordination bonds and coordination numbers become lower after introducing oxygen vacancies, which can contribute to more dangling bonding and better electrocatalytic performances. As expected, these oxygen vacancy-rich Co_3O_4 nanosheets showed a noticeable onset overpotential of about 220 mV (Fig. 3g), which is much lower than that of Co_3O_4. Besides, the oxygen vacancy-rich Co_3O_4 nanosheets displayed a small Tafel slope of 49.1 mV dec^{-1} (Fig. 3h), which is also lower than that of Co_3O_4. The improved OER performance and good long-term stability indicate that oxygen vacancies can indeed
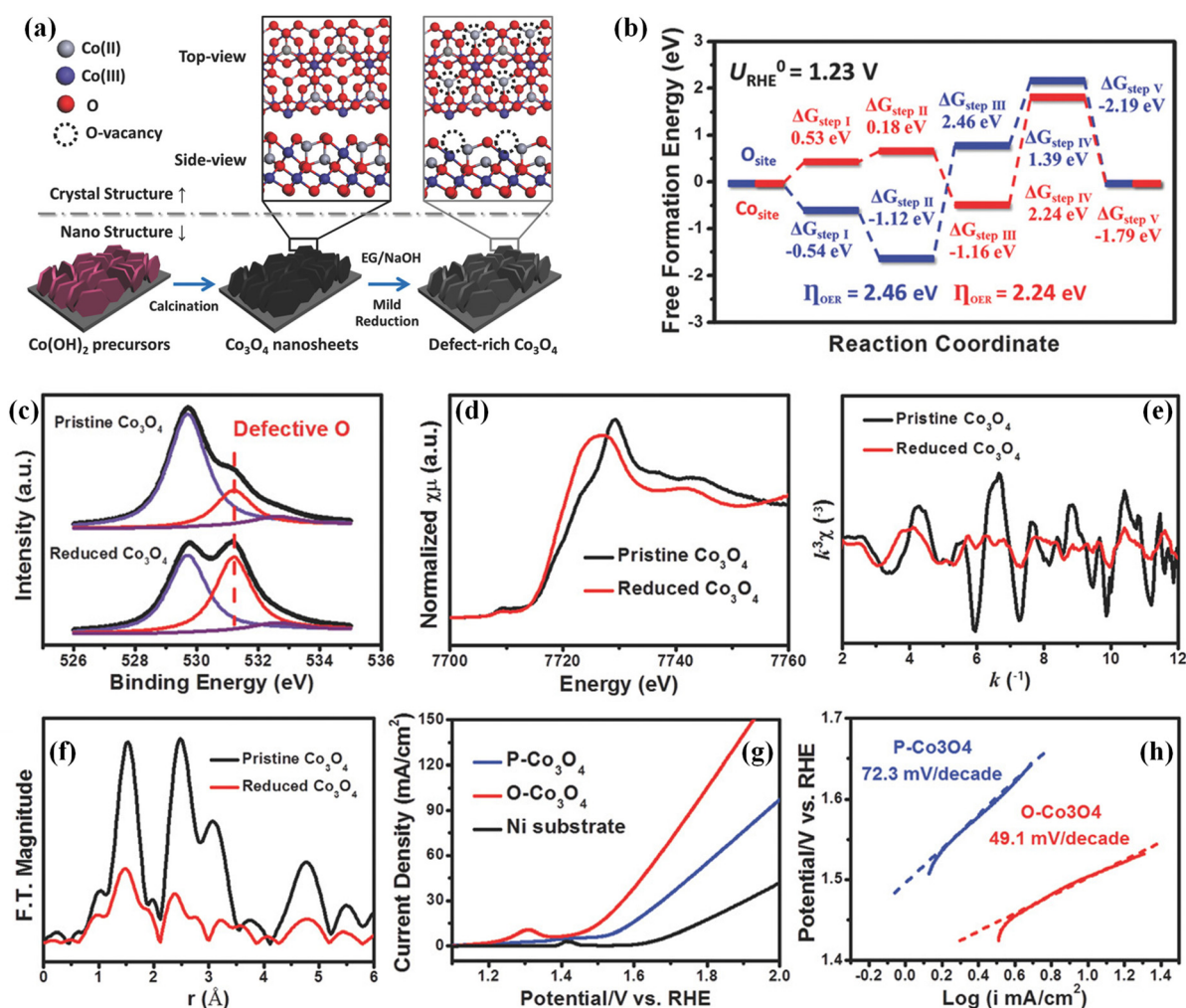

Fig. 3 (a) Schematic of preparing single crystalline Co_3O_4 nanosheets with oxygen vacancy defects. (b) Free energy diagram of Co_3O_4 and Co_3O_4 with oxygen vacancies for the OER. (c) O 1s XPS spectra of the obtained Co_3O_4 nanosheets and Co_3O_4 nanosheets with oxygen vacancy defects. (d) Co K-edge XANES spectra, (e) Co K-edge EXAFS spectra and (f) corresponding k^3-weighted Fourier-transformed pattern of Co_3O_4 nanosheets and Co_3O_4 nanosheets with oxygen vacancy defects. (g) LSV curves and (h) Tafel plots of the obtained Co_3O_4 nanosheets and Co_3O_4 nanosheets with oxygen vacancy defects. Copyright 2018, Wiley-VCH.[63]

enhance the intrinsic activity by regulating the electronic structures of Co_3O_4. In addition, Wang and co-workers introduced a large number of oxygen vacancies on Co_3O_4 nanosheets through using Ar radiofrequency plasma treatment.[64] The plasma treatment technology can also lead to the formation of rough surfaces and the obtained oxygen vacancies can optimize the electronic structures of Co_3O_4 electrocatalysts, which contributes to excellent activities and stabilities. Recently, vacancy defective electrocatalysts have attracted a lot of attention with high current density for practical applications. Yang's group prepared an Fe_2P–$WO_{2.92}$/NF electrode using an *in situ* growth method. The results confirmed that the electronic structures can be adjusted by introducing oxygen vacancies and the synergy between Fe_2P and $WO_{2.92}$, which can lead to large current density for the OER.[65] Despite all these, more useful strategies should be developed to introduce oxygen vacancies into transition metal-based (hydr)oxides for regulating their electronic structures and boosting their electrocatalytic performances.[66–70]

3.2 Metal cation vacancy defects

Metal cation vacancies is another kind of vacancy defect, which are similar to oxygen vacancies and can efficiently tune the electronic properties of transition metal-based (hydr)oxides electrocatalysts.[71–73] Although metal cation vacancies require higher formation energy than that for oxygen vacancies, enhancing the catalytic performances *via* introducing cation vacancies

has also been widely employed due to the rapid development of synthetic technologies. The efficient synthesis strategies for introducing metal cation vacancy defects into transition metal-based (hydr)oxide electrocatalysts are wet-chemistry strategies, high-temperature calcination treatment, and leaking metal cation strategies. For instance, Chen's group developed one room-temperature synthetic approach for preparing a cation vacancy-rich nanocrystalline $Co_xMn_{3−x}O_4$ electrocatalyst.[74] It was found that the spinel $Co_xMn_{3−x}O_4$ with metal cation (Co or Mn) vacancies displays optimized electronic structures, which leads to favorable oxygen-binding abilities and superior electrocatalytic OER performances. Zhang and co-workers reported a facile wet-chemistry strategy for growing Fe vacancy-rich ultrathin feroxyhyte (δ-FeOOH) nanosheets on Ni foam.[75] Fig. 4a displays the optimized crystalline structure of δ-FeOOH with Fe vacancies, and the reaction energy reveals that the generation of Fe cation vacancies is thermodynamically favorable. The SEM image in Fig. 4b shows the networked architecture feature of the as-prepared δ-FeOOH nanosheets. The TEM image (Fig. 4c) demonstrates that the nanosheets have an even thickness, and the HRTEM image (Fig. 4d) suggests exposure of the (001) faces of δ-FeOOH nanosheets and a thickness of about 1.9 nm. Fe K-edge XANES spectra in Fig. 4e show that the absorption edge of δ-FeOOH nanosheets upshifted, indicating the existence of Fe vacancies. The corresponding Fourier transforms (Fig. 4f) illustrate that the Fe–Fe shell in δ-FeOOH nanosheets is reduced to
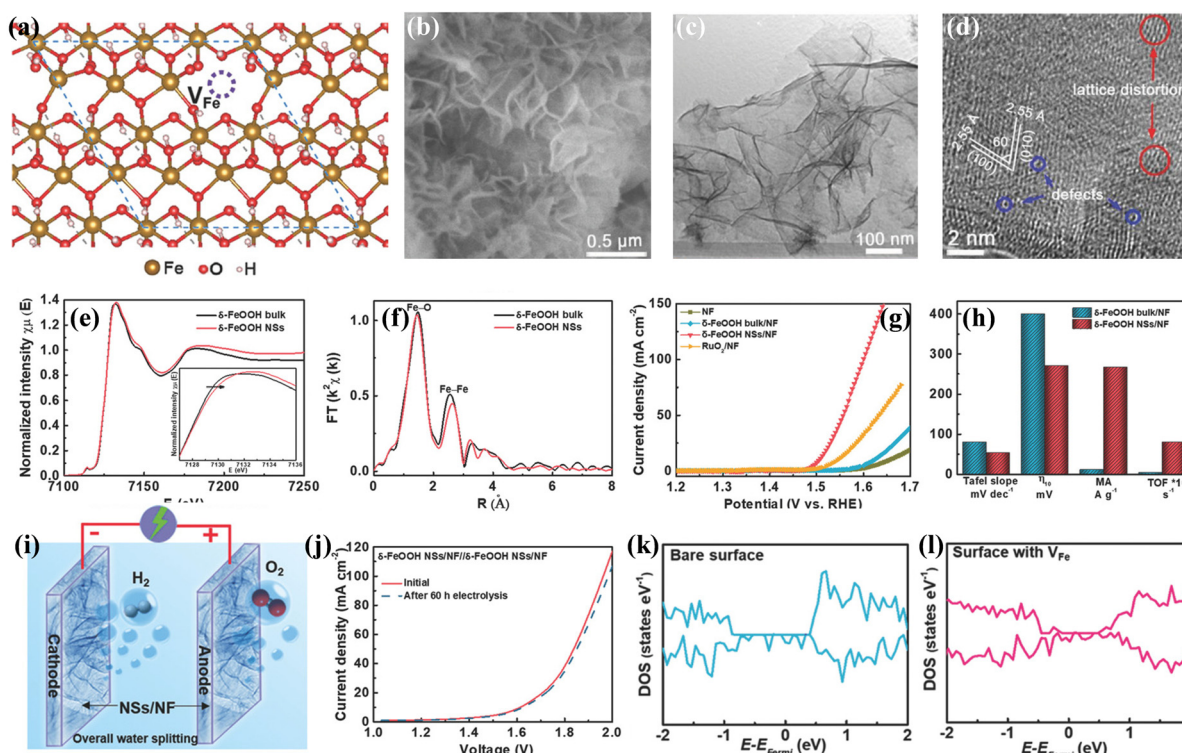

Fig. 4 (a) Crystalline structure of δ-FeOOH nanosheets with Fe vacancies. (b) SEM image, (c) TEM image and (d) HRTEM image of δ-FeOOH nanosheets with Fe vacancies. (e) Fe K-edge XANES spectrum and (f) the corresponding Fourier transform of the Fe K-edge EXAFS spectrum. (g) LSV curves for the OER 1.0 M KOH electrolyte. (h) Comparison of the OER performances over different electrocatalysts. (i) Schematic picture of water electrolysis cell and (j) LSV curve for overall water splitting. (k) Calculated DOS of δ-FeOOH without Fe vacancies, and (l) DOS of δ-FeOOH NSs with Fe vacancies. Copyright 2018, Wiley-VCH.[75]

1.6, further suggesting the formation of Fe vacancies. Notably, the δ-FeOOH nanosheets on Ni foam showed excellent OER performances (Fig. 4g and h) in 1 M KOH electrolyte. A low overpotential of 265 mV was required for δ-FeOOH nanosheets to achieve a current density of 10 mA cm^{-2}, which is much lower than that of δ-FeOOH bulk (400 mV). The Tafel slope of δ-FeOOH nanosheets was calculated to be 36 mV dec^{-1}, verifying its favourable kinetics. Moreover, the δ-FeOOH nanosheets also work well as HER electrocatalysts. Therefore, a two-electrode electrolyzer with δ-FeOOH nanosheets as both an anode and a cathode was constructed as shown in Fig. 4i. According to the LSV curve (Fig. 4j), only a small overpotential of 390 mV is needed to achieve a current density of 10 mA cm^{-2} for water splitting in the 1 M KOH electrolyte. After the stability test for 60 h, negligible decay can be detected on this δ-FeOOH nanosheets. The effect of Fe vacancies on electrocatalytic performances is explored *via* DFT calculations. The DOS of δ-FeOOH without and with Fe vacancies (Fig. 4k and l) reveals that the δ-FeOOH nanosheets without Fe vacancies possess a half-metal-like characteristic. After introducing Fe vacancies, the DOS is greatly increased near the Fermi level, suggesting that Fe vacancies can contribute to higher conductivity and faster charge transfer.

Besides, Zou's group fabricated $Co_{3-x}O_4$ electrocatalysts with Co cation vacancies *via* an *in situ* approach.[76] The Co K-edges XANES (Fig. 5a) clearly shows that Co-300 and Co-500 have higher oxidation states, suggesting the lower Co/O ratio caused by introducing Co cation vacancies. Fourier transforms in Fig. 5b reveal that Co-300 and Co-500 samples possess a lower Co coordination number, further demonstrating the existence of a large number of Co vacancies. As a result, the as-obtained $Co_{3-x}O_4$ with Co vacancies exhibited superior OER performances to Co_3O_4 (Fig. 5c) with a lower overpotential of 268 mV at 10 mA cm^{-2} and a smaller Tafel slope of 38.2 mV dec^{-1} in the KOH electrolyte. Besides, Co-300 showed a good durability for 10 000 seconds, and no obvious variations in Co-defect concentration were observed, suggesting that the cobalt defects are stable. To investigate the roles of Co cation
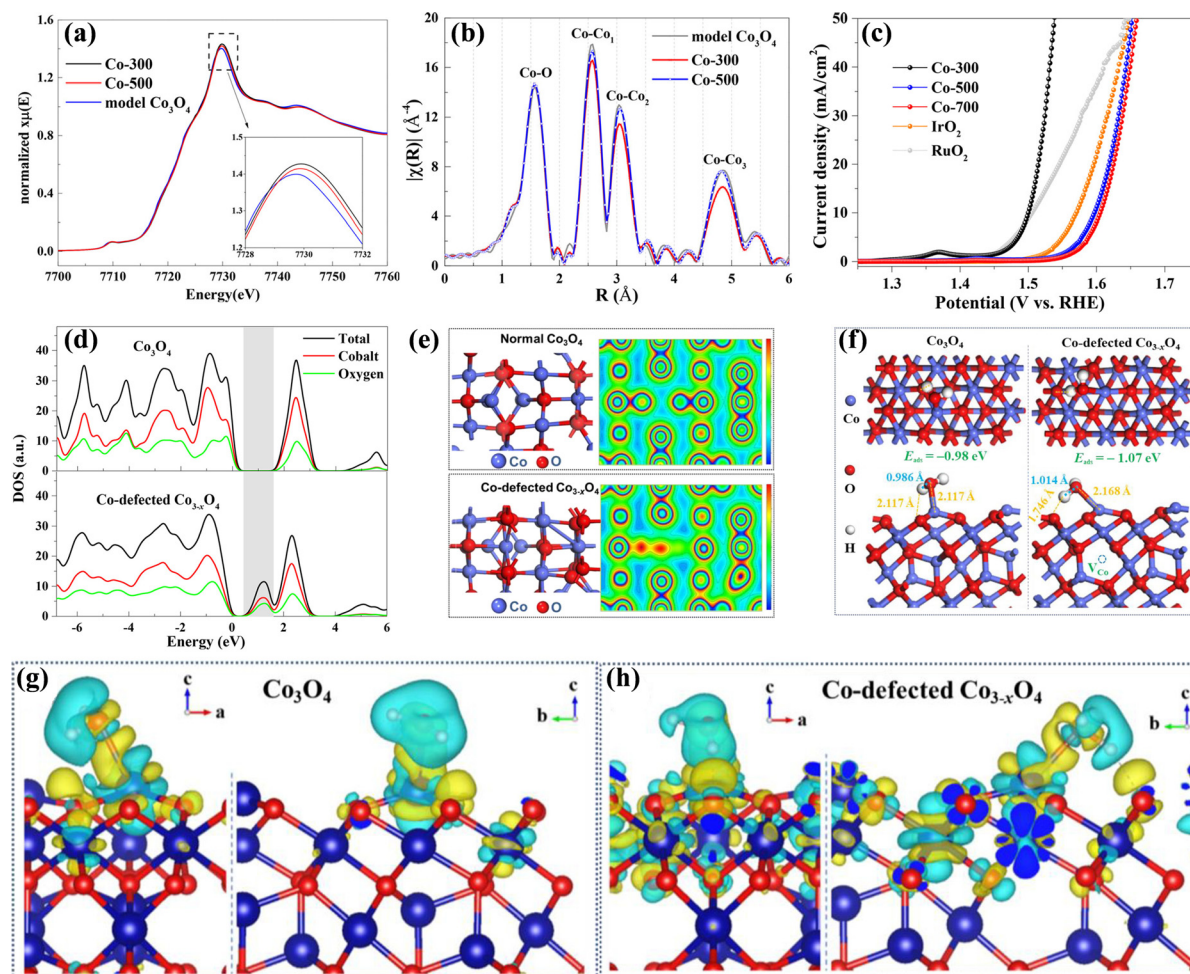

Fig. 5 (a) XANES and (b) corresponding Fourier transforms of Co-300, Co-500 and model Co_3O_4. (c) The LSV curves for the OER of Co-300, Co-500, Co-700, IrO_2 and RuO_2 samples. (d) TDOS and PDOS of Co_3O_4 and Co-defected $Co_{3-x}O_4$. (e) Optimized crystalline structures and charge density plots of Co_3O_4 and Co-defected $Co_{3-x}O_4$. (f) The configuration of H_2O adsorbed on Co_3O_4 and Co-defected $Co_{3-x}O_4$. (g) and (h) The charge density differences of H_2O adsorbed on Co_3O_4 and Co-defected $Co_{3-x}O_4$. Copyright 2018, American Chemical Society.[76]

vacancies in electrocatalytic performances, DFT calculation was carried out. As shown in Fig. 5d, the $Co_{3-x}O_4$ with Co vacancies has an increased DOS and a smaller band gap compared to Co_3O_4, suggesting that the conductivity is improved with Co vacancies. Fig. 5e and f uncover that Co vacancies could lead to distortion of neighboring atoms and cause electronic delocalization, which is beneficial to faster charge transport during reactions. Furthermore, the adsorption energy of H_2O over $Co_{3-x}O_4$ is -1.07 eV, lower than that over Co_3O_4 (-0.98 eV), indicating that Co vacancies can contribute to the adsorption of H_2O. Deformation charge density in Fig. 5g and h shows that $Co_{3-x}O_4$ has stronger interaction with adsorbed H_2O than Co_3O_4, suggesting that Co vacancy defects are beneficial to adsorption of H_2O and cleavage of H–OH bonds.

3.3 Multivacancy defects

According to the above discussion, oxygen vacancies and metal cation vacancies can play significant roles in tuning the electronic structures and enhancing electrocatalytic performances

of transition metal-based (hydr)oxide materials. It is reasonable to think that introducing multivacancies including oxygen vacancies and cation vacancies into one electrocatalyst is a highly efficient strategy for greatly improving its conductivity and electrocatalytic activity. In the past several years, many studies have reported that multivacancies can be employed as an efficient strategy for boosting the catalytic activities of (hydr)oxides. For creating multivacancy defects, the efficient synthesis strategies are the acid etching method, Ar plasma etching and so on. For example, Peng *et al.* reported a facile method (Fig. 6a) for introducing multivacancies (including Co, Fe and O vacancies) into CoFe LDHs to enhance the OER electrocatalytic performances.[77] The XRD patterns in Fig. 6b display that the phase information is not changed after acid etching. The intensities of diffraction peaks are decreased, indicating that the etching treatment can lead to the introduction of multivacancies. In Fourier transform of EXAFS for the Co K-edge (Fig. 6c), the intensities of Co–O and Co–Co/Fe peaks are slightly enhanced, suggesting that the interlayer space is
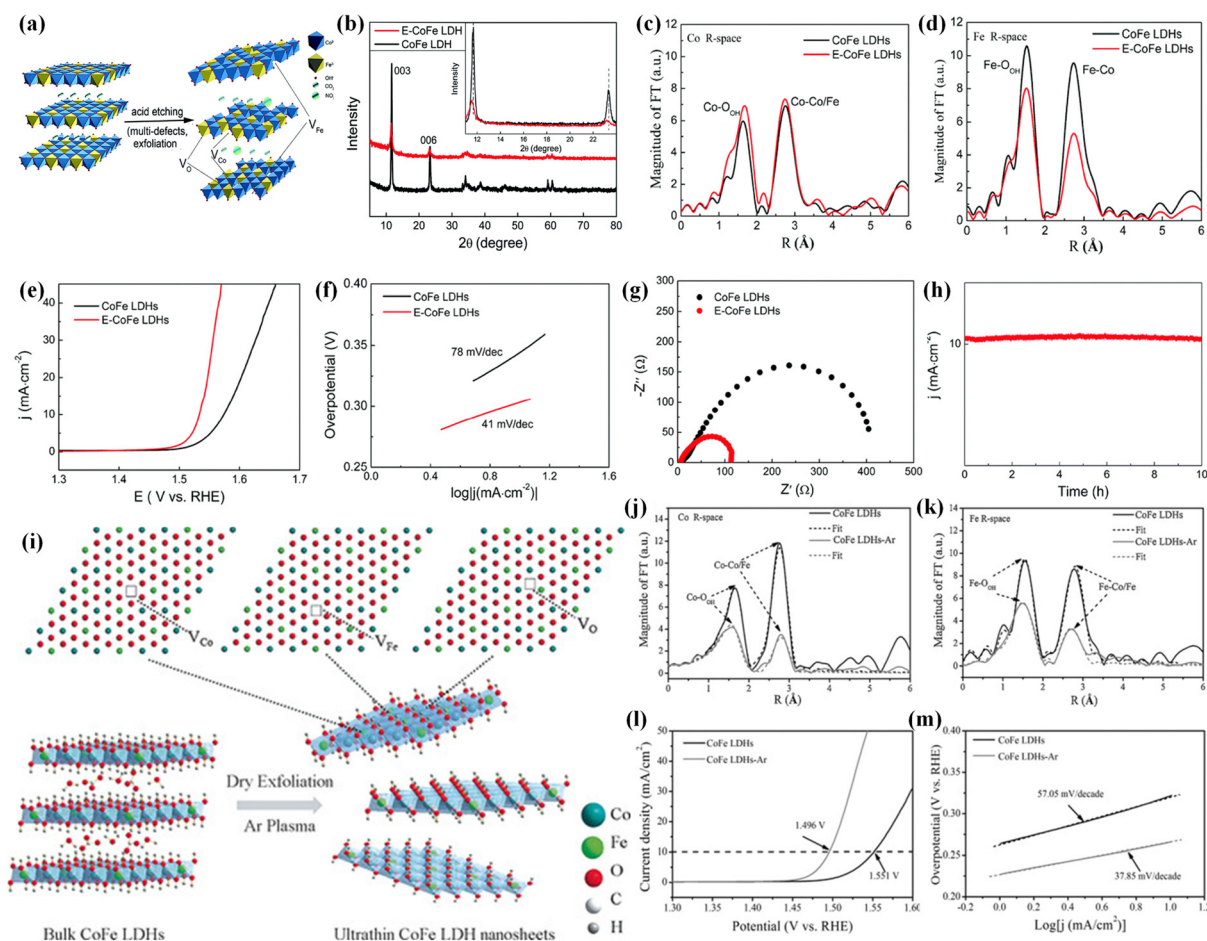

Fig. 6 (a) Schematic of creating Co, Fe and O vacancies in CoFe LDHs by the acid etching method. (b) XRD patterns of CoFe LDHs and CoFe LDHs with multiple defects. (c) and (d) Co and Fe K-edge Fourier transform magnitudes of k^3-weighted EXAFS spectra for CoFe LDHs and CoFe LDHs with Co, Fe and O vacancies. (e) The OER LSV curves, (f) Tafel plots and (g) Nyquist plots of CoFe LDHs and CoFe LDHs with multiple defects. (h) The stability of CoFe LDHs with multiple defects for the OER. Copyright 2017, Royal Society of Chemistry.[77] (i) Schematic for preparing CoFe LDH nanosheets with Co, Fe and O vacancies by Ar plasma exfoliation. (j) and (k) Fourier transforms of the Co and Fe edge XANES spectra. (l) LSV curves and (m) Tafel plots of CoFe LDH nanosheets and CoFe LDH nanosheets with Co, Fe and O vacancies for the OER in 1 M KOH. Copyright 2017, Wiley-VCH.[72]
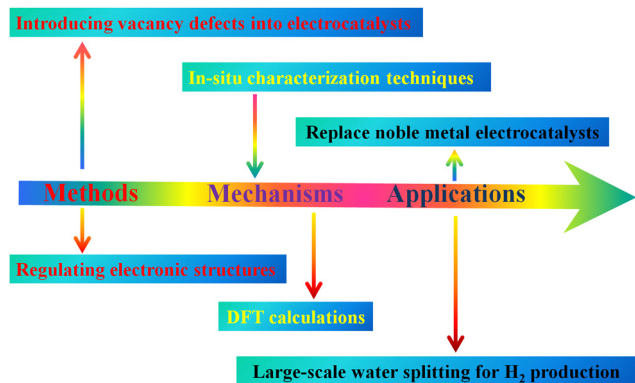
Fig. 7 Aspects on which attention should be focused for boosting the OER performances.

increased after acid etching treatment. In addition, the intensities of Fe–O and Fe–Co peaks shown in Fig. 6d largely decreased, demonstrating the existence of O vacancies and Fe vacancies. Remarkably, the as-synthesized CoFe LDHs with multivacancies displayed higher OER activities than CoFe LDHs. As shown in Fig. 6e, the potential to achieve a current density of 10 mA cm^{-2} over CoFe LDHs with multivacancies is 1.532 V, much lower than that over CoFe LDHs. Fig. 6f shows that the Tafel slope of CoFe LDHs with Co, Fe and O vacancies is about 41 mV dec^{-1}, which is also much smaller than that of CoFe LDHs. From the Nyquist plots in Fig. 6g, we can find that the CoFe LDHs with Co, Fe and O vacancies have lower charge transfer resistance than CoFe LDHs. Moreover, electrocatalytic performances can be maintained for at least 10 h over the CoFe LDHs with Co, Fe and O vacancies (Fig. 6h), which is benefited from altered morphology and electronic structures. Meanwhile, ultrathin CoFe LDHs nanosheets with multiple vacancies (including O, Co, and Fe vacancies) were fabricated by Yanyong *et al.* using the Ar plasma etching strategy (as shown in Fig. 6i).[72] The SEM images clearly show that the bulk CoFe LDHs are exfoliated into ultrathin LDH nanosheets by Ar plasma etching. The Fourier transforms of EXAFS (Fig. 6j and k) show that the CoFe LDH nanosheets with multivacancies have lower oscillation amplitude and a lower coordination number of Co (Fe)–O than CoFe LDHs, suggesting the formation of O vacancies, Co vacancies and Fe vacancies. The electrocatalytic OER performances in Fig. 6l and m manifest that CoFe LDH nanosheets with including O, Co, and Fe vacancies are more active (a lower overpotential of 266 mV at 10 mA cm^{-2} and a

smaller Tafel slope of 37.85 mV dec^{-1}) than CoFe LDH nanosheets. Remarkably, the CoFe LDH nanosheets can show negligible degradation after 2000 CV cycles. Moreover, a water-plasma-enabled exfoliation method was also reported to prepare the ultrathin CoFe LDH nanosheets with multivacancies (Co, Fe and O vacancies).[78]

4. Conclusions and outlook

In this review, three state-of-the-art defect-tuning strategies are summarized, including oxygen vacancy defects, metal cation vacancy defects and multivacancy defects, to regulate the electronic structures, improve the conductivity and boost the OER performances of transition metal (hydr)oxide-based electrocatalysts, which are crucial to develop efficient electrocatalysts for water splitting. The regulated electronic structures of transition metal (hydr)oxide-based electrocatalysts by introducing defects can greatly improve the conductivity, resulting in an optimized adsorption ability with intermediates and a lowered reaction energy barrier of the OER. Although defect-tuning strategies open a new avenue for boosting the electrocatalytic performances of low-cost transition metal (hydr)oxide-based nanomaterials, making them promising candidates for replacing noble metal catalysts for large-scale electrochemical water splitting is still a big challenge. As shown in Fig. 7, several challenging aspects on which attention should be focused are listed.

(i) Introducing stable vacancy defects into electrocatalysts using facile methods is the chief task. As mentioned above, defects can regulate their electronic structures, which can work well as a powerful strategy for boosting the OER performance of transition metal-based (hydr)oxides (Table 3). However, synthesizing ideal electrocatalysts to replace noble metals for the OER is still a big challenge. Thus, more efficient strategies should be developed to introduce stable vacancy defects into the OER electrocatalysts to further enhance their electrocatalytic performances.

(ii) Fundamental investigation of the electronic structure–property relationship and electrocatalytic mechanism is necessary, which provides guidance for synthesizing novel advanced electrocatalysts or optimizing the existing electrocatalysts for the OER. However, accurately exploring the structure–property relationship and electrocatalytic mechanism is still one challenging issue. At present, DFT calculations combined with advanced *in situ* characterization techniques are promising methods to explore the electrocatalytic mechanism.[79–85] For example, *in situ*

Table 3 OER performances of different vacancy defect regulated electrocatalysts

Defects	Catalysts	Electrolyte	Overpotential at 10 mA cm^{-2}	Tafel slope (mV dec^{-1})	Stability (h)	Ref.
Oxygen vacancy defect	Reduced Co$_3$O$_4$	1 M KOH	—	72	1.67	60
	O–Co$_3$O$_4$	1 M KOH	—	49.1	15	63
	CoO$_x$-4 h	1 M KOH	306	67	2.78	1
Metal cation vacancy defect	δ-FeOOH NSs/NF	1 M KOH	108	68	60	75
	Co-300	1 M KOH	268	38.2	2.78	76
	NiAl$_\delta$P	1 M KOH	256	76	—	79
Multivacancy defect	CoFe LDHs–Ar	1 M KOH	266	37.85	2000 cv	72
	E-CoFe LDHs	1 M KOH	300	41	10	77

Raman spectroscopy, XAS, and isotope labelling experiments, could give atomic-level insights into the reaction mechanism.

(iii) Replacing the as-prepared electrocatalysts with noble metal-based electrocatalysts is also very urgent for large-scale water splitting. To meet the requirements for practical application, the as-prepared electrocatalysts with defects should have the following characteristics: (1) excellent durability in harsh electrolytes and under high potential conditions, enabling electrocatalysts to possess a long-term working life; (2) excellent electronic conductivity that facilitates electron transfer during the electrocatalytic reaction; (3) appropriate adsorption ability that contributes to the adsorption and desorption of intermediates; (4) low cost and environmental friendliness, which are crucial for large-scale application.

Conflicts of interest

There are no conflicts to declare.

Acknowledgements

Notes and references

1 W. Xu, F. Lyu, Y. Bai, A. Gao, J. Feng, Z. Cai and Y. Yin, Porous cobalt oxide nanoplates enriched with oxygen vacancies for oxygen evolution reaction, *Nano Energy*, 2018, **43**, 110–116.

2 A. Kubacka, M. F. Garcia and G. Colon, Advanced nanoarchitectures for solar photocatalytic applications, *Chem. Rev.*, 2012, **112**, 1555–1614.

3 B. Wang, C. Tang, H. F. Wang, X. Chen, R. Gao and Q. Zhang, Core-branch CoNi hydroxysulfides with versatilely regulated electronic and surface structures for superior oxygen evolution electrocatalysis, *J. Energy Chem.*, 2019, **38**, 8–14.

4 X. Zou and Y. Zhang, Noble metal-free hydrogen evolution catalysts for water splitting, *Chem. Soc. Rev.*, 2015, **44**, 5148–5180.

5 W. Wang, Z. Wang, Y. Hu, Y. Liu and S. Chen, A potential-driven switch of activity promotion mode for the oxygen evolution reaction at Co_3O_4/NiO_xH_y interface, *eScience*, 2022, **2**, 438–444.

6 Y. Yan, B. Xia, Z. Xu and X. Wang, Recent development of molybdenum sulfides as advanced electrocatalysts for hydrogen evolution reaction, *ACS Catal.*, 2014, **4**, 1693–1705.

7 X. Y. Lu, W. L. Yim, B. H. R. Suryanto and C. Zhao, Electrocatalytic oxygen evolution at surface-oxidized multiwall carbon nanotubes, *J. Am. Chem. Soc.*, 2015, **137**, 2901–2907.

8 X. X. Zou, J. Su, R. Silva, A. Goswami, B. R. Sathe and T. Asefa, Efficient oxygen evolution reaction catalyzed by low-density Ni-doped Co_3O_4 nanomaterials derived from metal-embedded graphitic C_3N_4, *Chem. Commun.*, 2013, **49**, 7522–7524.

9 W. J. Zhou, X. J. Wu, X. H. Cao, X. Huang, C. L. Tan, J. Tian, H. Liu, J. Y. Wang and H. Zhang, Ni_3S_2 nanorods/Ni foam composite electrode with low overpotential for electrocatalytic oxygen evolution, *Energy Environ. Sci.*, 2013, **6**, 2921–2924.

10 C. Z. Yuan, Y. F. Jiang, Z. Wang, X. Xie, Z. K. Yang, A. B. Yousaf and A. W. Xu, Cobalt phosphate nanoparticles decorated with nitrogen-doped carbon layers as highly active and stable electrocatalysts for the oxygen evolution reaction, *J. Mater. Chem. A*, 2016, **4**, 8155–8160.

11 J. Zhu, L. S. Hu, P. X. Zhao, L. Y. S. Lee and K. Y. Wong, Recent advances in electrocatalytic hydrogen evolution using nanoparticles, *Chem. Rev.*, 2020, **120**, 851–918.

12 M. R. Gao, W. C. Sheng, Z. B. Zhuang, Q. R. Fang, S. Gu, J. Jiang and Y. S. Yan, Efficient water oxidation using nanostructured α-nickel-hydroxide as an electrocatalyst, *J. Am. Chem. Soc.*, 2014, **136**, 7077–7084.

13 Y. Jiao, Y. Zheng, M. Jaroniec and S. Z. Qiao, Design of electrocatalysts for oxygen-and hydrogen-involving energy conversion reactions, *Chem. Soc. Rev.*, 2015, **44**, 2060–2086.

14 Q. Z. Xu, Y. Z. Su, H. Wu, H. Cheng, Y. P. Guo, N. Li and Z. Q. Liu, Effect of morphology of Co_3O_4 for oxygen evolution reaction in alkaline water electrolysis, *Curr. Nanosci.*, 2015, **11**, 107–112.

15 H. J. Wang, Z. G. Li, G. H. Li, F. Peng and H. Yu, Co_3S_4/NCNTs: a catalyst for oxygen evolution reaction, *Catal. Today*, 2015, **245**, 74–78.

16 M. R. Gao, X. Cao, Q. Gao, Y. F. Xu, Y. R. Zheng, J. Jiang and S. H. Yu, Nitrogen-Doped Graphene Supported $CoSe_2$ Nanobelt Composite Catalyst for Efficient Water Oxidation, *ACS Nano*, 2014, **8**, 3970–3978.

17 Y. J. Bai, H. J. Zhang, Y. Y. Feng, L. Fang and Y. Wang, Sandwich-like CoP/C nanocomposites as efficient and stable oxygen evolution catalysts, *J. Mater. Chem. A*, 2016, **4**, 9072–9079.

18 Z. H. Xiao, X. B. Huang, L. Xu, D. F. Yan, J. Huo and S. Y. Wang, Edge-selectively phosphorus-doped few-layer graphene as an efficient metal-free electrocatalyst for the oxygen evolution reaction, *Chem. Commun.*, 2016, **52**, 13008–13011.

19 R. Wei, M. Fang, G. Dong, C. Lan, L. Shu, H. Zhang, X. Bu and J. C. Ho, High-Index Faceted Porous Co_3O_4 Nanosheets with Oxygen Vacancies for Highly Efficient Water Oxidation, *ACS Appl. Mater. Interfaces*, 2018, **10**, 7079–7086.

20 G. S. Hutchings, Y. Zhang, J. Li, B. T. Yonemoto, X. Zhou, K. Zhu and F. Jiao, In Situ Formation of Cobalt Oxide

Nanocubanes as Efficient Oxygen Evolution Catalysts, *J. Am. Chem. Soc.*, 2015, **137**, 4223–4229.

21 X. M. Liu, X. Cui, K. Dastafkan, H. F. Wang, C. Tang, C. Zhao, A. Chen, C. He, M. Han and Q. Zhang, Recent advances in spinel-type electrocatalysts for bifunctional oxygen reduction and oxygen evolution reactions, *J. Energy Chem.*, 2021, **53**, 290–302.

22 Y. Tong, H. Mao, Y. Xu and J. Liu, Oxygen vacancies confined in Co_3O_4 quantum dots for promoting oxygen evolution electrocatalysis, *Inorg. Chem. Front.*, 2019, **6**, 2055–2060.

23 Y. Y. Liang, Y. G. Li, H. L. Wang, J. G. Zhou, J. Wang, T. Regier and H. J. Dai, Co_3O_4 nanocrystals on graphene as a synergistic catalyst for oxygen reduction reaction, *Nat. Mater.*, 2011, **10**, 780–786.

24 C. Z. Yuan, K. S. Hui, H. Yin, S. Zhu, J. Zhang, X. L. Wu, X. Hong, W. Zhou, X. Fan, F. Bin, F. Chen and K. N. Hui, Regulating intrinsic electronic structures of transition-metal-based catalysts and the potential applications for electrocatalytic water splitting, *ACS Mater. Lett.*, 2021, **3**, 752–780.

25 Y. Shi and B. Zhang, Recent advances in transition metal phosphide nanomaterials: synthesis and applications in hydrogen evolution reaction, *Chem. Soc. Rev.*, 2016, **45**, 1529–1541.

26 P. C. K. Vesborg, B. Seger and I. J. Chorkendorff, Recent development in hydrogen evolution reaction catalysts and their practical implementation, *Phys. Chem. Lett.*, 2015, **6**, 951–957.

27 Y. P. Zhu, X. Xu, H. Su, Y. P. Liu, T. Chen and Z. Y. Yuan, Ultrafine Metal Phosphide Nanocrystals in Situ Decorated on Highly Porous Heteroatom-Doped Carbons for Active Electrocatalytic Hydrogen Evolution, *ACS Appl. Mater. Interfaces*, 2015, **7**, 28369–28376.

28 M. Xiao, Y. Miao, Y. Tian and Y. Yan, Synthesizing nanoparticles of Co-P-Se compounds as electrocatalysts for the hydrogen evolution reaction, *Electrochim. Acta*, 2015, **165**, 206–210.

29 C. Xie, D. F. Yan, W. Chen, Y. Q. Zou, R. Chen, S. Q. Zang, Y. Y. Wang, X. D. Yao and S. Y. Wang, Insight into the design of defect electrocatalysts: from electronic structure to adsorption energy, *Mater. Today*, 2019, **31**, 47–68.

30 Y. C. Yao, S. L. Hu, W. X. Chen, Z. Q. Huang, W. C. Wei, T. Yao, R. R. Liu, K. T. Zang, X. Q. Wang, G. Wu, W. J. Yuan, T. W. Yuan, B. Q. Zhu, W. Liu, Z. J. Li, D. S. He, Z. G. Xue, Y. Wang, X. S. Zheng, J. C. Dong, C. R. Chang, Y. X. Chen, X. Hong, J. Luo, S. Q. Wei, W. X. Li, P. Strasser, Y. E. Wu and Y. D. Li, Engineering the electronic structure of single atom Ru sites via compressive strain boosts acidic water oxidation electrocatalysis, *Nat. Catal.*, 2019, **2**, 304–313.

31 J. R. Feng, F. Lv, W. Y. Zhang, P. H. Li, K. Wang, C. Yang, B. Wang, Y. Yang, J. H. Zhou, F. Lin, G. C. Wang and S. J. Guo, Iridium-based multimetallic porous hollow nanocrystals for efficient overall-water-splitting catalysis, *Adv. Mater.*, 2017, **29**, 1703798.

32 X. Rong, J. Parolin and A. M. Kolpak, A fundamental relationship between reaction mechanism and stability in

33 E. Fabbri, A. Habereder, K. Waltar, R. Kötz and T. J. Schmidt, Developments and perspectives of oxide-based catalysts for the oxygen evolution reaction, *Catal. Sci. Technol.*, 2014, **4**, 3800–3821.

34 J. O. M. Bockris, Kinetics of activation controlled consecutive electrochemical reactions: anodic evolution of oxygen, *J. Chem. Phys.*, 1956, **24**, 817–827.

35 A. I. Krasil'shchkov, Intermediate stages of oxygen anodic evolution, *Zh. Fiz. Khim.*, 1963, **37**, 273.

36 W. E. O'Grady, C. Iwakura, J. Huang and E. Yeager, in *Ruthenium oxide catalysts for the oxygen electrode*, ed. M. W. Breiter, The Electrochemical Society, Princeton, 1974, p. 286.

37 W. E. O'Grady, C. Iwakura and E. Yeager, *Oxygen electrocatalysts for life support systems*, American Society of Mechanical Engineers, 1976, p. 76-ENAs-37.

38 J. O. M. Bockris and T. Otagawa, The electrocatalysis of oxygen evolution on perovskites, *J. Electrochem. Soc.*, 1984, **131**, 290–302.

39 I. C. Man, H. Y. Su, F. Calle-Vallejo, H. A. Hansen, J. I. Martínez, N. G. Inoglu, J. Kitchin, T. F. Jaramillo, J. K. Nørskov and J. Rossmeisl, Universality in oxygen evolution electrocatalysis on oxide surfaces, *ChemCatChem*, 2011, **3**, 1159–1165.

40 W. H. Wade and N. Hackerman, Anodic phenomena at an iron electrode, *Trans. Faraday Soc.*, 1957, **53**, 1636–1647.

41 J. Y. Li, W. L. Zhou, X. Zhao, W. Cheng, H. Su, H. Zhang, M. Liu and Q. Liu, Donutlike RuCu nanoalloy with ultrahigh mass activity for efficient and robust oxygen evolution in acid solution, *ACS Appl. Energy Mater.*, 2019, **2**, 7483–7489.

42 H. Jin, J. Joo, N. K. Chaudhari, S. I. Choi and K. Lee, Recent progress in bifunctional electrocatalysts for overall water splitting under acidic conditions, *ChemElectroChem*, 2019, **6**, 3244–3253.

43 L. Li, H. Yang, J. Miao, L. Zhang, H. Y. Wang, Z. Zeng, W. Huang, X. Dong and B. Liu, Unraveling oxygen evolution reaction on carbon-based electrocatalysts: effect of oxygen doping on adsorption of oxygenated intermediates, *ACS Energy Lett.*, 2017, **2**, 294–300.

44 E. Fabbri, M. Nachtegaal, T. Binninger, X. Cheng, B. J. Kim, J. Durst, F. Bozza, T. Graule, R. Schäublin, L. Wiles, M. Pertoso, N. Danilovic, K. E. Ayers and T. J. Schmidt, Dynamic surface self-reconstruction is the key of highly active perovskite nano-electrocatalysts for water splitting, *Nat. Mater.*, 2017, **16**, 925–931.

45 H. Y. Wang, S. F. Hung, H. Y. Chen, T. S. Chan, H. M. Chen and B. Liu, In Operando Identification of Geometrical-Site-Dependent Water Oxidation Activity of Spinel Co_3O_4, *J. Am. Chem. Soc.*, 2016, **138**, 36–39.

46 H. Y. Wang, S. F. Hung, Y. Y. Hsu, L. Zhang, J. Miao, T. S. Chan, Q. Xiong and B. Liu, In Situ Spectroscopic Identification of μ-OO Bridging on Spinel Co_3O_4 Water Oxidation Electrocatalyst, *J. Phys. Chem. Lett.*, 2016, **7**, 4847–4853.

47 H. Y. Wang, Y. Y. Hsu, R. Chen, T. S. Chan, H. M. Chen and B. Liu, Ni^{3+}-Induced Formation of Active NiOOH on the

metal oxide catalysts for oxygen evolution, *ACS Catal.*, 2016, **6**, 1153–1158.

Spinel Ni–Co Oxide Surface for Efficient Oxygen Evolution Reaction, *Adv. Energy Mater.*, 2015, **5**, 1500091.

48 R. Chen, H. Y. Wang, J. Miao, H. Yang and B. Liu, A flexible high-performance oxygen evolution electrode with three-dimensional $NiCo_2O_4$ core-shell nanowires, *Nano Energy*, 2015, **11**, 333–340.

49 R. Chen, G. Sun, C. Yang, L. Zhang, J. Miao, H. Tao, H. Yang, J. Chen, P. Chen and B. Liu, Achieving stable and efficient water oxidation by incorporating NiFe layered double hydroxide nanoparticles into aligned carbon nanotubes, *Nanoscale Horiz.*, 2016, **1**, 156–160.

50 K. Zhu, H. Liu, M. Li, X. Li, J. Wang, X. Zhu and W. Yang, Atomic-scale topochemical preparation of crystalline Fe^{3+}-doped β-Ni(OH)$_2$ for an ultrahigh-rate oxygen evolution reaction, *J. Mater. Chem. A*, 2017, **5**, 7753–7758.

51 Y. Sun, C. Liu, D. C. Grauer, J. Yano, J. R. Long, P. Yang and C. J. Chang, Electrodeposited cobalt-sulfide catalyst for electrochemical and photoelectrochemical hydrogen generation from water, *J. Am. Chem. Soc.*, 2013, **135**, 17699–17702.

52 C. G. Morales-Guio and X. Hu, Amorphous molybdenum sulfides as hydrogen evolution catalysts, *Acc. Chem. Res.*, 2014, **47**, 2671–2681.

53 G. Wu, W. Chen, X. Zheng, D. He, Y. Luo, X. Wang, J. Yang, Y. Wu, W. Yan, Z. Zhuang, X. Hong and Y. Li, Hierarchical Fe-doped NiO_x nanotubes assembled from ultrathin nanosheets containing trivalent nickel for oxygen evolution reaction, *Nano Energy*, 2017, **38**, 167–174.

54 A. Indra, P. W. Menezes, N. R. Sahraie, A. Bergmann, C. Das, M. Tallarida, D. Schmeißer, P. Strasser and M. Driess, Unification of catalytic water oxidation and oxygen reduction reactions: amorphous beat crystalline cobalt iron oxides, *J. Am. Chem. Soc.*, 2014, **136**, 17530–17536.

55 J. Huang, J. Chen, T. Yao, J. He, S. Jiang, Z. Sun, Q. Liu, W. Cheng, F. Hu, Y. Jiang, Z. Pan and S. Wei, CoOOH nanosheets with high mass activity for water oxidation, *Angew. Chem., Int. Ed.*, 2015, **127**, 8846–8851.

56 H. Wang, H. W. Lee, Y. Deng, Z. Lu, P. C. Hsu, Y. Liu, D. Lin and Y. Cui, Bifunctional non-noble metal oxide nanoparticle electrocatalysts through lithium-induced conversion for overall water splitting, *Nat. Commun.*, 2015, **6**, 7261.

57 L. Wei, H. E. Karahan, S. Zhai, H. Liu, X. Chen, Z. Zhou, Y. Lei, Z. Liu and Y. Chen, Amorphous bimetallic oxide–graphene hybrids as bifunctional oxygen electrocatalysts for rechargeable Zn–air batteries, *Adv. Mater.*, 2017, **29**, 1701410.

58 S. Zhou, X. Miao, X. Zhao, C. Ma, Y. Qiu, Z. Hu, J. Zhao, L. Shi and J. Zeng, Engineering electrocatalytic activity in nanosized perovskite cobaltite through surface spin-state transition, *Nat. Commun.*, 2016, **7**, 11510.

59 S. Dou, L. Tao, R. Wang, S. El Hankari, R. Chen and S. Wang, Plasma-assisted synthesis and surface modification of electrode materials for renewable energy, *Adv. Mater.*, 2018, **30**, e1705850.

60 Y. Wang, T. Zhou, K. Jiang, P. Da, Z. Peng, J. Tang, B. Kong, W. B. Cai, Z. Yang and G. Zheng, Reduced Mesoporous Co_3O_4 Nanowires as Efficient Water Oxidation Electrocatalysts and Supercapacitor Electrodes, *Adv. Energy Mater.*, 2014, **4**, 1400696.

61 L. Zhuang, L. Ge, Y. Yang, M. Li, Y. Jia, X. Yao and Z. Zhu, Bimetal-Organic Framework Derived $CoFe_2O_4$/C Porous Hybrid Nanorod Arrays as High-Performance Electrocatalysts for Oxygen Evolution Reaction, *Adv. Mater.*, 2017, **29**, 1604437.

62 C. Zhu, S. Fu, D. Du and Y. Lin, Facilely Tuning Porous NiCo2O4 Nanosheets with Metal Valence-State Alteration and Abundant Oxygen Vacancies as Robust Electrocatalysts Towards Water Splitting, *Chem. – Eur. J.*, 2016, **22**, 4000–4007.

63 Z. Cai, Y. Bi, E. Hu, W. Liu, N. Dwarica, Y. Tian, X. Li, Y. Kuang, Y. Li, X. Q. Yang, H. Wang and X. Sun, Single-Crystalline Ultrathin Co_3O_4 Nanosheets with Massive Vacancy Defects for Enhanced Electrocatalysis, *Adv. Energy Mater.*, 2018, **8**, 1701694.

64 L. Xu, Q. Jiang, Z. Xiao, X. Li, J. Huo, S. Wang and L. Dai, Plasma-Engraved Co3O4 Nanosheets with Oxygen Vacancies and High Surface Area for the Oxygen Evolution Reaction, *Angew. Chem., Int. Ed.*, 2016, **128**, 5363–5367.

65 Q. Peng, Q. He, Y. Hu, T. T. Isimjan, R. Hou and X. Yang, Interface engineering of porous Fe_2P-$WO_{2.92}$ catalyst with oxygenvacancies for highly active and stable large-current oxygen evolution and overall water splitting, *J. Energy Chem.*, 2022, **65**, 574–582.

66 S. Dou, L. Tao, J. Huo, S. Wang and L. Dai, Etched and doped Co_9S_8/graphene hybrid for oxygen electrocatalysis, *Energy Environ. Sci.*, 2016, **9**, 1320–1326.

67 J. Bao, X. Zhang, B. Fan, J. Zhang, M. Zhou, W. Yang, X. Hu, H. Wang, B. Pan and Y. Xie, Ultrathin spinel-structured nanosheets rich in oxygen deficiencies for enhanced electrocatalytic water oxidation, *Angew. Chem., Int. Ed.*, 2015, **127**, 7507–7512.

68 T. Ling, D. Y. Yan, Y. Jiao, H. Wang, Y. Zheng, X. Zheng, J. Mao, X. W. Du, Z. Hu, M. Jaroniec and S. Z. Qiao, Engineering surface atomic structure of single-crystal cobalt (II) oxide nanorods for superior electrocatalysis, *Nat. Commun.*, 2016, **7**, 12876.

69 Q. Xu, H. Jiang, H. Zhang, H. Jiang and C. Li, Phosphorus-driven mesoporous Co_3O_4 nanosheets with tunable oxygen vacancies for the enhanced oxygen evolution reaction, *Electrochim. Acta*, 2018, **259**, 962–967.

70 Y. Zhou, C. K. Dong, L. L. Han, J. Yang and X. W. Du, Top-down preparation of active cobalt oxide catalyst, *ACS Catal.*, 2016, **6**, 6699–6703.

71 Y. Liu, H. Cheng, M. Lyu, S. Fan, Q. Liu, W. Zhang, Y. Zhi, C. Wang, C. Xiao and S. Wei, Low Overpotential in Vacancy-Rich Ultrathin $CoSe_2$ Nanosheets for Water Oxidation, *J. Am. Chem. Soc.*, 2014, **136**, 15670–15675.

72 Y. Wang, Y. Zhang, Z. Liu, C. Xie, S. Feng, D. Liu, M. Shao and S. Wang, Layered double hydroxide nanosheets with multiple vacancies obtained by dry exfoliation as highly efficient oxygen evolution electrocatalysts, *Angew. Chem., Int. Ed.*, 2017, **56**, 5867–5871.

73 J. Zhu, Z. Ren, S. Du, Y. Xie, J. Wu, H. Meng, Y. Xue and H. Fu, Co-vacancy-rich $Co_{1-x}S$ nanosheets anchored on rGO for high-efficiency oxygen evolution, *Nano Res.*, 2017, **10**, 1819–1831.

74 F. Cheng, J. Shen, B. Peng, Y. Pan, Z. Tao and J. Chen, Rapid room-temperature synthesis of nanocrystalline spinels as

oxygen reduction and evolution electrocatalysts, *Nat. Chem.*, 2011, **3**, 79–84.

75 B. Liu, Y. Wang, H. Q. Peng, R. Yang, Z. Jiang, X. T. Zhou, C. S. Lee, H. J. Zhao and W. J. Zhang, Iron vacancies induced bifunctionality in ultrathin feroxyhyte nanosheets for overall water splitting, *Adv. Mater.*, 2018, **30**, 1803144.

76 R. Zhang, Y. C. Zhang, L. Pan, G. Q. Shen, N. Mahmood, Y. H. Ma, Y. Shi, W. Jia, L. Wang, X. Zhang, W. Xu and J. J. Zou, Engineering cobalt defects in cobalt oxide for highly efficient electrocatalytic oxygen evolution, *ACS Catal.*, 2018, **8**, 3803–3811.

77 P. Zhou, Y. Y. Wang, C. Xie, C. Chen, H. W. Liu, R. Chen, J. Huo and S. Y. Wang, Acid-etched layered double hydroxides with rich defects for enhancing the oxygen evolution reaction, *Chem. Commun.*, 2017, **53**, 11778–11781.

78 R. Liu, Y. Wang, D. Liu, Y. Zou and S. Wang, Water-plasma-enabled exfoliation of ultrathin layered double hydroxide nanosheets with multivacancies for water oxidation, *Adv. Mater.*, 2017, **29**, 1701546.

79 W. Cheng, H. Zhang, X. Zhao, H. Su, F. Tang, J. Tian and Q. Liu, A metal-vacancy-solid-solution NiAlP nanowall array bifunctional electrocatalyst for exceptional all-pH overall water splitting, *J. Mater. Chem. A*, 2018, **6**, 9420–9427.

80 X. Zheng, P. De Luna, F. P. García de Arquer, B. Zhang, N. Becknell, M. B. Ross, Y. Li, M. N. Banis, Y. Li, M. Liu, O. Voznyy, C. T. Dinh, T. Zhuang, P. Stadler, Y. Cui, X. Du, P. Yang and E. H. Sargent, Sulfur-modulated tin sites enable highly selective electrochemical reduction of CO$_2$ to formate, *Joule*, 2017, **4**, 794–805.

81 H. Yang, S. Hung, S. Liu, K. Yuan, S. Miao, L. Zhang, X. Huang, H. Wang, W. Cai, R. Chen, J. Gao, X. Yang, W. Chen, Y. Huang, H. Chen, C. Li, T. Zhang and B. Liu, Atomically dispersed Ni (i) as the active site for electrochemical CO$_2$ reduction, *Nat. Energy*, 2018, **3**, 140–147.

82 X. Li, W. Bi, M. Chen, Y. Sun, H. Ju, W. Yan, J. Zhu, X. Wu, W. Chu, C. Wu and Y. Xie, Exclusive Ni–N$_4$ Sites Realize Near-Unity CO Selectivity for Electrochemical CO$_2$ Reduction, *J. Am. Chem. Soc.*, 2017, **139**, 14889–14892.

83 M. Gorlin, P. Chernev, J. F. de Araujo, T. Reier, S. Dresp, B. Paul, R. Krahnert, H. Dau and P. Strasser, Oxygen evolution reaction dynamics, faradaic charge efficiency, and the active metal redox states of Ni–Fe oxide water splitting electrocatalysts, *J. Am. Chem. Soc.*, 2016, **138**, 5603–5614.

84 H. Mistry, A. S. Varela, C. S. Bonifacio, I. Zegkinoglou, I. Sinev, Y. W. Choi, K. Kisslinger, E. A. Stach, J. C. Yang, P. Strasser and B. R. Cuenya, Highly selective plasma-activated copper catalysts for carbon dioxide reduction to ethylene, *Nat. Commun.*, 2016, **7**, 12123.

85 Y. Jiao, Y. Zheng, K. Davey and S. Z. Qiao, Activity origin and catalyst design principles for electrocatalytic hydrogen evolution on heteroatom-doped graphene, *Nat. Energy*, 2016, **1**, 16130.